Article

Facile Synthesis of Magnetic Biochar Derived from Burley Tobacco Stems towards Enhanced Cr(VI) Removal: Performance and Mechanism

Baihui Cui [1,2,3]**, Zhihua Chen** [4]**, Feihua Wang** [1]**, Zihan Zhang** [1]**, Yanran Dai** [1]**, Dabin Guo** [2,3]**, Wei Liang** [1,]*** and Yu Liu** [2,5]

[1] Institute of Hydrobiology, Chinese Academy of Sciences, Wuhan 430072, China; cuibaihui0306@163.com (B.C.); wangfeihua93@ihb.ac.cn (F.W.); zihanzhang1018@gmail.com (Z.Z.); yanrandai@ihb.ac.cn (Y.D.)

[2] Advanced Environmental Biotechnology Centre, Nanyang Environment & Water Research Institute, Nanyang Technological University, Singapore 637141, Singapore; guodabin2018@gmail.com (D.G.); CYliu@ntu.edu.sg (Y.L.)

[3] School of Civil Engineering, Guangzhou University, Guangzhou 510006, China

[4] Key Laboratory for Yellow River and Huai River Water Environment and Pollution Control, School of Environment, Henan Normal University, Xinxiang 453007, China; chenzhihua@htu.edu.cn

[5] School of Civil and Environmental Engineering, Nanyang Technological University, Singapore 639798, Singapore

*** Correspondence: liangwei02@tsinghua.org.cn or Wliang@ihb.ac.cn

Abstract: In this study, ferric-loaded magnetic burley tobacco stem biochar (MBTS) was synthesized via pyrolysis to improve the removal of Cr(VI). The results showed that MBTS had an adsorption capacity of 54.92 mg Cr(VI)/g, which was about 14 times higher than raw burley tobacco stem biochar (i.e., 3.84 mg/g). According to the findings obtained, a three-step mechanism of Cr(VI) removal by MBTS was further put forward, i.e., (1) Cr(VI) exchanged with hydroxyl groups on MBTS, (2) the reduction in Cr(VI) to Cr(III) mediated by oxygen-containing groups, and (3) the chelation of produced Cr(III) with the amino groups on MBTS. FTIR spectra further revealed that C-N, C-H, and C=C groups played an important role in Cr(VI) removal. Furthermore, the adsorption equilibrium and kinetics of Cr(VI) on MBTS could better be described by the Langmuir equation and pseudo-second-order rate equation. This study clearly demonstrated that ferric-loaded biochar derived from burley tobacco stems could serve as a cost-effective magnetic adsorbent for the high-efficiency removal of soluble Cr(VI) from wastewater. Tobacco stem-adsorbed Cr(VI) realized a green path for treating waste by waste.

Keywords: magnetic biochar; Cr(VI) removal; Cr(III) immobilization; mechanism analysis

1. Introduction

Heavy metals are assorted as one of a multitude of toxic materials in wastewater, which is of great significance to investigate its removal. Chromium (Cr) has been considered as one of the most hazardous wastewater metal pollutants due to its advanced mobility, solubility, and toxicity. Chromium (Cr) mainly exists in two patterns, i.e., hexavalent chromium (Cr(VI)) and trivalent chromium (Cr(III)), with excessive hazards caused by Cr(VI) than Cr(III) [1]. Cr(VI) exists widely in various industrial activities, such as metal electroplating, dyeing, tanneries, fertilizer, metallurgy, and fungicide production, and possesses a high solubility when entering into the aquatic environment [2]. It should be noted that it is indispensable to bring down the concentration of Cr(VI) as low as possibly reasonable before discharging. In view of this, various methods have been widely used for Cr(VI) removal, such as adsorption, biological degradation, chemical precipitation, reverse osmosis, ion exchange, and membrane separation [3]. Adsorption is largely applied

among these, for its high-efficiency, environmentally friendly, operation-flexibility and low-cost [4,5].

Biochar is a pyrogenic black carbon acquiring increasing attention in recent years, which could be produced from biomass under oxygen-limited conditions [6,7]. Biochar was being developed as a good choice of low-cost sorbent with unique properties, especially the modified biochar, e.g., relatively large surface area [8], excellent ion exchange capacity, easy modification to support functional groups, and a range of chemical compositions [9]. Moreover, compared with other sorbents, biochar shows a great affinity for kinds of chromium, due to its surface heterogeneity, abundant porous structure or functional groups [10,11]. In addition, biochar has a negatively charged surface, specific ligands, acidic oxygen groups, and basic nitrogen groups, which is beneficial for the removal of Cr(VI) [12–14].

Biochar could be derived from a great variety of waste biomasses or by-products of agriculture, which are relatively inexpensive and more economically and environmentally [15–17]. China's tobacco production ranks first in the world. As reported, the leaf output of Chinese tobacco could achieve 2,325,000 tons in 2014 [18]. Meanwhile, tobacco waste, mainly tobacco stems, reach 3–5 million tons per year [19]. Tobacco stems (TSs) produced abound from the tobacco yard, but they just act as a tobacco residue. The tobacco stem is the major residue of tobacco in the field and causes significant harm to the subsequent crops. Consequently, the convenient way to remove them from the field is by burning or landfills, which also cause serious pollution to the air, soil, and other environmental problems [20]. Thus, it is an environmentally friendly way to obtain biochar from tobacco straw for the sake of treating waste with waste and for the potential use for chromium removal. The modification of the biochar could enhance its metal adsorption capacity through various physical and chemical methods, e.g., surface oxidation, acid activation, and steam activation [21,22]. In addition, biochar is generally prepared in powder, posing a challenge for separation [23]. In this regard, the potential solution is to educe the biochar with a magnetic feature, depending on the magnetic separation characteristic [24]. Additionally, magnetic modification could also add the affinity with Cr anions through chemical adsorption. Ferric complex is regarded as a better choice to modify the biochar for chromium removal [25]. Moreover, the discharge of Cr(III) that results from the reduction in Cr(VI) is another challenge, and amine groups complexed with Cr(III) ions could enhance Cr(III) immobilization [26]. To the author's knowledge, the biochar derived from tobacco stems with amine groups and modified by Fe_3O_4 magnetic particles for chromium removal have rarely been reported.

Biochar derived from tobacco stems (BTSs) was modified with $FeCl_3$ magnetic particle and applied for Cr(VI) removal in this study. Tobacco stem biochar could offer binding sites for anion Cr(VI) adsorption, and Fe_3O_4 particle modification induced more binding sites. In addition, ferric particles posed magnetic properties to the biochar, which benefit for its separation. The objectives of the present study are (i) to characterize the physicochemical properties of the magnetic biochar (MBTS); (ii) to explore the amine groups that act as the new binding site for Cr(III) removal; and (iii) to assess the potential Cr(VI) removal characteristics and the mechanism by the novel magnetic biochar.

2. Materials and Methods

2.1. Synthesis of MBTS Magnetic Biochar

A burley tobacco stem was obtained from Hubei Province (China). The TS was air-dried, crushed, and then sieved into 0.25 mm (60 mesh) with an electric pulverize in 30,000 r/min. $FeCl_3 \cdot 6H_2O$ (analytical reagent) together with TS via Fe/TS (m/m) = 0.5 ratio was dissolved in 100 mL deionized water at 100 °C for 6 h, and then dried in an air-cyclic oven (80 °C, 24 h) to acquire the MBTS precursor. The tobacco stem without $FeCl_3 \cdot 6H_2O$, as well as impregnation with hot water (100 °C) for 6 h (BTS precursor), was used for parallel experiments. The MBTS was pyrolyzed at 400 °C for 30 min, which was raised from 25 °C at a certain rate of 10 °C/min. In the meantime, N_2 of 99.99% purity was continuously passed through the quartz cylindrical funnel at a rate of 100 mL/min. Then, this was stored in a

vacuum (0.1 atm) cooling to room temperature naturally. In order to remove appendiculate impurities, MBTS was washed with ethyl alcohol and distilled water, then dried under 80 °C for 24 h in an air circulated drying oven. Biochar derived from the raw tobacco stem without disposing of $FeCl_3 \cdot 6H_2O$ (BTS) was acquired in the same programmed condition.

2.2. Batch Adsorptions

The stock Cr(VI) solution (1 g/L) was preconditioned by dissolving $K_2Cr_2O_7$ (analytical reagent) into deionized water. All desirable concentrations (30, 40, 50, 60, 70, 80, 90, 100, 150 mg/L) of Cr(VI) solutions were acquired by diluting the prepared stock solution. Then, 20 mg MBTS and BTS was added into 20 mL reaction Cr(VI) solution. Adjust with 0.1 M NaOH and 0.1 M HCl to obtain the desired pH value of the solution. Subsequently, the solution was automatically shaken at 120 rpm under 25, 35, and 45 °C separately. Kinetic experiments were executed at 25 °C, Cr(VI) 30–150 mg/L, and pH = 3.0. After the reaction, the solution was filtered through a 0.22 μm filter, and the collected filtrate was then measured using UV-Vis spectrophotometry (V-5800H, Thermo) at λ = 540 nm. Finally, the adsorption capacity (qt, mg/g) of Cr(VI) can be calculated as the following Equation:

$$qt = \frac{(Co - Ct)}{m} \tag{1}$$

where C_o and C_t are the concentration of Cr(VI) at initial and time, t, mg/L; m is the adsorbent dose (g/L). The separated MBTS after adsorption was dried under 80 °C for 6 h in an air-cyclic dried oven for the further characterization.

The adsorption amount experiment of BTS and MBTS at 298 K separately was performed, and the adsorption data were described by the Langmuir model, which then acquired the maximum capacity.

2.3. Characterization of MBTS

The surface morphology and pore size of BTS and MBTS were inspected by the Brunauer–Emmet–Teller (BET, Anton Paar, U.S.A., Quadrasorb SI MP 21) specific surface area analyzer, which depended on the adsorption and desorption of nitrogen, using 250 mg BTS or MBTS under 250 °C dried and degassed for 12 h under the N_2 condition. The micromorphology of MBTS was analyzed with the field emission scanning electron microscope (FESEM/EDS, JEOL JSM-7200F with Oxford Aztec Standard X-max80), with a working voltage of 10.0 kV in the pressure of 1.9×10^{-4} Pa. For evaluating the interaction mechanism, X-ray diffraction (XRD, Holland, Philips, PANAnalytical B.V.) patterns were analyzed at a Cu Kα radiation (λ = 1.54178 Å, V = 40 Kv, I = 40 mA), with scanning 2θ from 10° to 80° at 17°/min. The Fourier transform infrared (FTIR, Shimadzu IR Prestige-21) spectrum was taken to analyze the functional groups of BTS and MBTS. Chemical valences of C1s, N1s, O1s, Fe2P, and Cr2P and ion exchange mechanisms were carried out by X-ray photoelectron spectroscopy (XPS, U.K., Kratos AXIS Supra).

2.4. Adsorption Kinetics and Isotherms

Adsorption kinetics were applied for simulating the adsorption rate, and the kinetics of the Cr(VI) adsorption was fitted by two universal models as follows:
Pseudo-First-Order Model (PFO Model)

$$Ln(q_e - q_t) = Lnq_e - k_1 t \tag{2}$$

Pseudo-Second-Order Model (PSO Model)

$$t/q_t = 1/k_2 q_e^2 + t/q_e \tag{3}$$

where q_e and q_t are respective adsorption capacities at equilibrium and time t (mg/g); t is the adsorption time (min); k_1 and k_2 are separately first- and second-order rates.

In this study, three adsorption isotherm models were adopted to analyze the adsorption equilibrium data, which are the Langmuir, Freundlich, and Sips isotherms. (Equations (4)–(6)).

$$\text{Langmuir model}: \quad q_e = \frac{K_L q_{max} C_e}{1 + K_L C_e} \tag{4}$$

$$\text{Freundlich model}: \quad q_e = K_F C_e^{1/n_F} \tag{5}$$

$$\text{Sips isotherms}: \quad q_e = \frac{q_{max}(K_g C_e)^{n_L}}{1 + (K_g C_e)^{n_L}} \tag{6}$$

where q_e represents the Cr(VI) metal ion amount adsorbed at equilibrium, mg/g; Ce represents the equilibrium Cr(VI) concentration, mol/L; q_{max} represents the saturation adsorption capacity, mg/g; K represents the Langmuir constant, L/mg; K_F is interrelated to the relative adsorption constant, $(mg/g)/(mol/L)^{1/n}$; $K_g(L/mol)$ represents the constant of Sips isotherms.; and $1/n_F$ and n_L represent the dimensionless exponents of Freundlich and Sips isotherms separately.

3. Results and Discussion

3.1. Characterization of the Synthesized Biochar

The surface morphology and chemical composition of MBTS and BTS were analyzed with SEM-EDS (Figure 1). It was found that that BTS had a relatively smooth sheet shape without the presence of nanoparticles, while MBTS exhibited a rough carbon sheet shape with particles uniformly loaded on its surface (Figure 1b). Figure 1d further reveals a polyhedral structure adhering to the MBTS with the obvious presence of ferric oxides nanoparticles [27]. This was supported by the XRD results showing Fe_3O_4 or γ-Fe_2O_3 being the main crystalline in MBTS. According to the EDS images (Figure 1d), C, N, O, Fe, and Cl are the four primary elements in MBTS. Furthermore, the crystalline structure adhered to the MBTS, which was mainly constituted with elements of Fe and O, calculating the exist of ferric oxides.
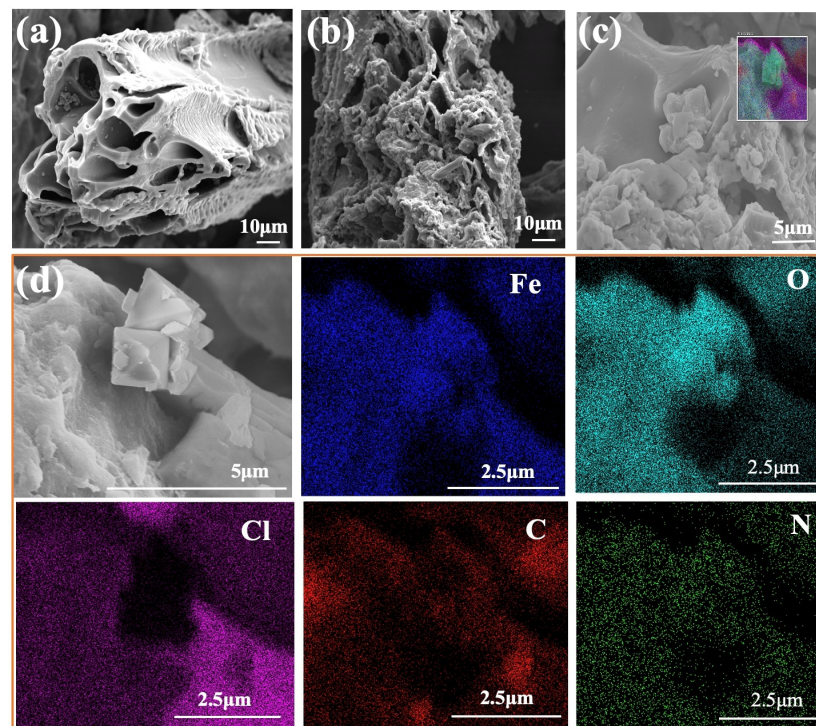

Figure 1. Scanning electron microscopic images. (**a**): BTS; (**b**): MBTS; (**c**): EDS images of MBTS; and (**d**): insert Figure 1c.

Table 1 shows the BET analysis of BTS and MBTS. It can be observed that the S_{BET} of MBTS was estimated to be 4.33 m^2/g, which was significantly smaller than that of BTS (i.e., 32.78 m^2/g), while the total pore volume of MBTS (i.e., 0.008 cm^3/g) was also much lower than that of BTS (i.e., 0.072 cm^3/g). It should also be noted that the average pore radius of both MBTS and BTS were comparable. The pore of BTS was originally large and became smaller as a result of being blocked by ferric after being modified, and then the pores became larger with the dissolving ferric with the acidic solution during the Cr(VI) adsorption experiment. However, unlike from BTS, the analysis reveals that MBTS is highly rich in various functional groups.

Table 1. BET characteristics of modified and pristine biochar.

Adsorbent	BET Surface Area (m^2/g)	Total Pore Volume (cm^3/g)	Average Pore Radius (nm)
BTS	32.78	0.072	1.631
MBTS before adsorption	4.33	0.008	1.633
MBTS after adsorption	13.83	0.039	1.637

To further verify the existential form of magnetic iron oxide, the BTS and MBTS materials were characterized by XRD before and after adsorption separately. Figure 2a shows that, except for a slight diffraction peak at 26.7 °C, no obvious peak can be detected for BTS, implying the turbostratic crystallites formatted in BTS [28]. XRD showed that the MBTS and MBTS + Cr may contain Fe_3O_4 or γ-Fe_2O_3. The formation of iron compounds may pose an important influence on Cr(VI) removal. Furthermore, the after-adsorption pattern (i.e., MBTS + Cr pattern) contains Fe_3O_4 or γ-Fe_2O_3, demonstrating that the material remains magnetic after adsorption, which is convenient for magnetic separation after adsorption. The surface functional groups of MBTS were analyzed by FTIR. Figure 2b reveals the FTIR data for the BTS, MBTS, and MBTS with adsorbed Cr(VI). The peak at 1039 cm^{-1} and 1314 cm^{-1} was concerning to the C-N group [29,30], and the peak at 1539 cm^{-1} was correlated with the C=C group. Compared with BTS, the new peaks at 781 cm^{-1} and 874 cm^{-1} in FTIR spectra of MBTS, which are in line with the C–H stretching vibration, reveal chemical interactions between MBTS surface and $FeCl_3$ [29]. After the biochar was modified with $FeCl_3$, a new peak at 572 cm^{-1} conforming with the ferric oxide (Fe_3O_4 or γ-Fe_2O_3) was presented in the spectra of MBTS, indicating that the tobacco stem biochar was successfully modified with $FeCl_3$, which is in accordance with the XRD characterization result. As for the MBTS adsorbed Cr spectra, the peak of nearly 580 cm^{-1} conforms with the representative Fe–O vibration [31], which that after the adsorption of Cr(VI) by the ferric oxides on MBTS, a redox reaction occurred, which reduced Cr(VI) to Cr(III), while the chemical valence of iron changed, then and Fe–O vibration occurred. Figure 2c shows that MBTS disperses in a water suspension and can be magnetically separated.
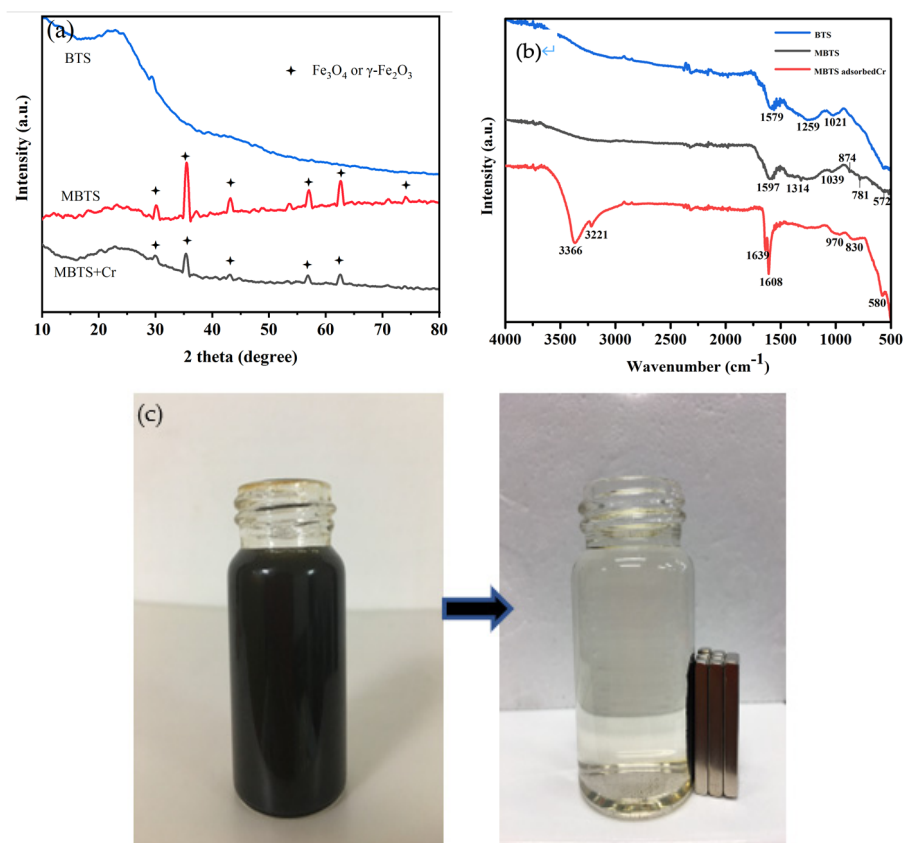
Figure 2. (**a**) The XRD patterns of BTS and MBTS, (**b**) FTIR of MBTS, and (**c**) MBTS dispersed in a water suspension and being magnetically separated.

3.2. Adsorption Isotherm and Kinetics

The isotherm data of Cr(VI) adsorption on MBTS were fitted to the Langmuir, Freundlich, and Sips isotherm equations (Figure 3). It appears from Table 2 that the Langmuir and Sips isotherms present a better description for the adsorption data than the Freundlich isotherm. The Sips isotherm can be reasonably simplified to the Langmuir isotherm when the n_L value approximates to the unity [32]. The maximum capacity of Cr(VI) adsorption on BTS and MBTS was determined to be 3.84 mg/g and 58.74 mg/g, respectively, at 298 K, which are higher than some reported biochar and magnetic biochar adsorbents listed in Table 3.

Table 2. Adsorption isotherms of Cr(VI) on MBTS.

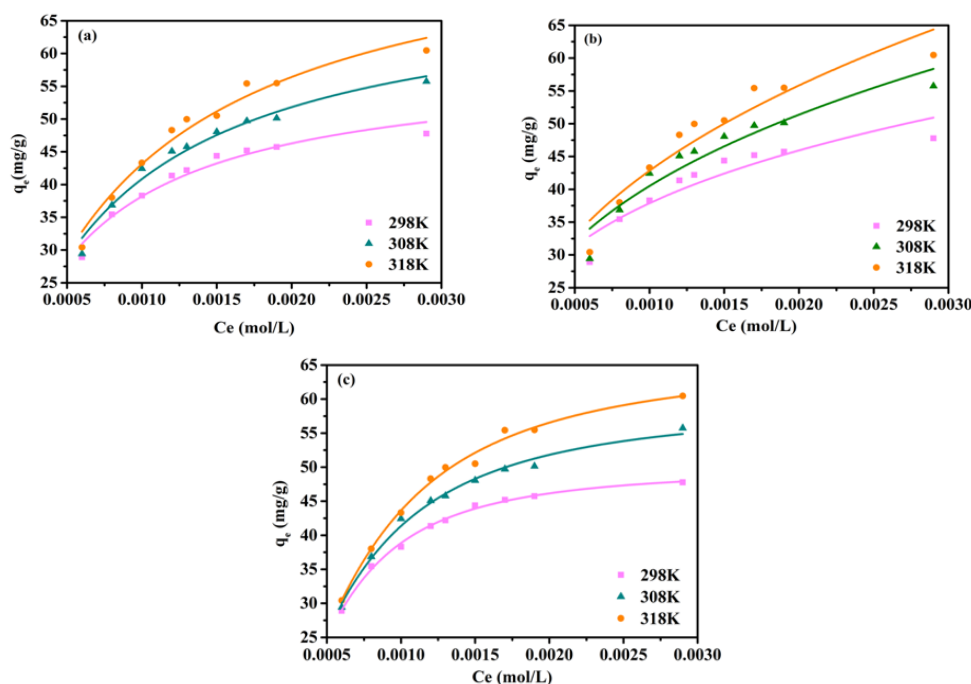|	T(K)	q_m (mg/g)	K_L (L/mol)	K_f ((mg/g)/ $(mol/L)^{1/n}$)	K_g (L/mol)	R^2	$1/n_F$	n_L
Langmuir model	298	58.74	1856.77			0.959		
	308	70.89	1358.20			0.973		
	318	70.89	1121.19			0.970		
Freundlich model	298			258.66		0.860	0.28	
	308			433.26		0.903	0.34	
	318			602.06		0.900	0.38	
Sips isotherm	298	49.83			1998.19	0.996		1.83
	308	59.24			1692.24	0.990		1.59
	318	65.97			1512.75	0.991		1.62

Figure 3. The qt-Ct profiles in the adsorption of Cr(VI) on MBTS at different temperatures. (**a**) Prediction by the Langmuir model; (**b**) Freundlich model; and (**c**) Sips isotherm.

Table 3. Comparisons of adsorption capacities of Cr(VI) ions on biochar and magnetic biochar with reported adsorbents.

Absorbent	Modified Method	q_m (mg/g)	Reference
BTS	Biochar derived from tobacco stems	3.84	This study
MBTS	BTS modified with $FeCl_3$	54.92	This study
PBC-ND	Biochar derived from bamboo and poplar	5.4	[33]
Fe/PBC-ND	PBC-ND modified with $Fe(NO_3)_3$	25.68	[33]
BM-Fe-HC	Biochar modified with $FeCl_3$	48.1	[34]
PC	Porous carbon	2.50	[35]
Fe@PC	PC modified with $Fe(NO_3)_3$	10.07	[35]
Magnetic biochar	Biochar modified with FeCl3	27.2	[28]

Based on the adsorption equilibrium constants determined from the Langmuir isotherm (Table 2), the adsorption thermodynamics were studied by using the following Equations:

$$\Delta G^0 = -RT\ln K_e \tag{7}$$

$$\ln K_e = \frac{\triangle S^0}{R} - \frac{\triangle H^0}{RT} \tag{8}$$

where K_e means the equilibrium constant of thermodynamic, which approximates the Langmuir equilibrium constant for a diluted solution [36]; $\Delta G°$ denominates the change of free energy, kJ/mol; R signifies the gas constant (8.314 J/(mol K)); T expresses the absolute temperature, K; and $\Delta S°$ (J/(mol K)) and $\Delta H°$ (kJ/mol) verbalize the change of entropy and enthalpy, separately.

As shown in Table 4, the negative ΔG^0 evinced the Cr(VI) adsorption on the MBTS was spontaneous, while both the ΔH^0 value (i.e., 2.842 kJ/mol) and $\Delta S°$ value (i.e., 9.903 KJ/mol) were positive, which indicated an endothermic adsorption process [37].

Table 4. Thermodynamics parameters for Cr(VI) adsorption.

Adsorbent	ΔH^0 (KJ/mol)	ΔS^0 (J/mol K)	ΔG^0 (KJ/mol)		
			298 K	308 K	318 K
MBTS	2.842	9.903	−0.109	−0.208	−0.307

It appears from Figure 4 that the experimental data could be better depicted by the PSO rate equation. This also showed a chemisorption of Cr(VI) by MBTS. In the light of the above Cr(VI) adsorption behaviors on the MBTS samples, we investigated the contact time to Cr(VI) adsorption on MBTS in diverse Cr(VI) initial concentrations extending from 30 mg/L to 150 mg/L, by using the same MBTS dosage (20 mg/50 mL). The influence of removal time on Cr(VI) adsorption (Figure 4a) illustrates that distinct outset concentrations show identical adsorption laws, and the removal efficiency reduces with the initial enhancement in the Cr(VI) concentration. Figure 4a also reveals the residual Cr(VI) concentration ($R_c = C_t/C_0$) with different contact times (t, min). The adsorption rates of Cr(VI) in MBTS were considerably fast at the beginning of the contact time, and no obvious further reduction was measured with the increasing adsorption time after 750 min, inferring that the adsorption of Cr(VI) by MBTS was a chemical process. The kinetics in the adsorption procedure was determined from the curve fitting with the PFO and the PSO. The corresponding detailed kinetic parameters were determined out from the adsorption kinetics. The coefficient value calculated from the PSO model ($R^2 = 0.993$) was higher than that of the PFO model ($R^2 = 0.904$). The PSO model fitted the adsorption kinetics better between the two kinetic models, demonstrating that the rate-controlling mechanism for the Cr(VI) adsorption on MBTS is chemisorption.
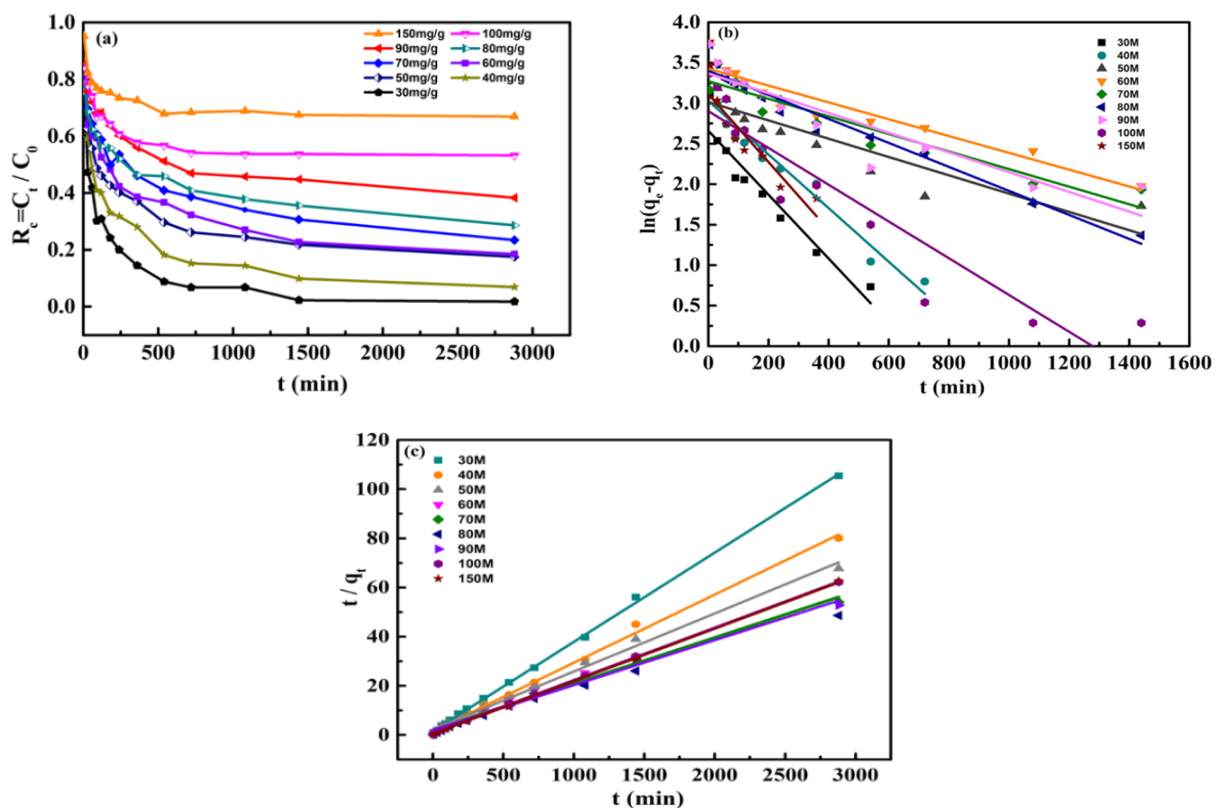

Figure 4. The removal of Cr(VI) on MBTS results for: (**a**) removal efficiencies of different initial concentration versus time; (**b**) PFO linear plots; and (**c**) PSO linear plots. pHCr(VI) = 3.0 ± 0.1, T = 298 ± 1 K.

3.3. Effect of pH on the Adsorption of Cr(VI) on MBTS

The pH (1–9) of the solution on the adsorption of Cr(VI) by MBTS was also surveyed under conditions of initial concentration 50 mg/L, dosage 1 g/L, and 24 h contact time. Figure 5 reveals that the Cr(VI) adsorption on MBTS clearly increased at pH = 1.0–3.0 and gradually decreased with the increasing pH, which was consistent with the previous research [38,39]. The maximum adsorption of Cr(VI) on MBTS occurred at a pH of 3. As previously presented in the research, at pH < 2, Cr(VI) mainly existed as $Cr_2O_7^{2-}$, at pH 2–6, both $Cr_2O_7^{2-}$ and $HCrO_4^-$ were retained, and CrO_4^{2-} became dominant when pH < 6 [28,40]. As we know, Cr(VI) was negatively charged and the surface of MBTS was protonated in an acidic environment, showing a positive charge. Therefore, electrostatic attraction was critical in adsorbing the Cr(VI) ion. Whereas, in alkaline or neutral conditions, the surface of MBTS was deprotonated and presented a neutral or negative charge, so the removal efficiency decreased consequently owing to the electrostatic repulsion.
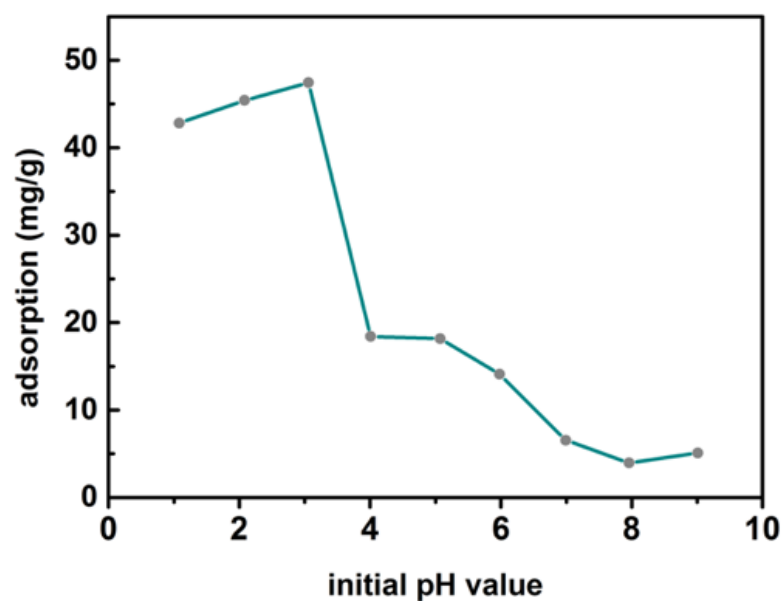

Figure 5. Effect of pH on the Cr(VI) removal.

3.4. Effect of Coexisting Ions

Moreover, Cr(VI) ions inescapably coexist with diverse electrolyte ions in wastewater, which might power the movement of pollutants. Usually, Na^+, Ca^{2+}, and K^+ as well as Cl^-, SO_4^{2-}, and NO_3^- were chosen as the common coexisting ions. Figure 6 describes the impacts of different ions on Cr(VI) (50 mg/L concentration) removal; we found that the coexistence of diverse ions reduced the adsorption ability of Cr(VI) on MBTS. Additionally, the great majority of coexisting ions posed no distinct effect on the Cr(VI) adsorption. In particular, SO_4^{2-} had more negative impacts on Cr(VI) removal than MBTS, presumably due to SO_4^{2-} both competing for adsorption sites with Cr(VI) and complexation with the Fe ion [41]. Ca^{2+} in solution was adsorbed on the MBTS and competed with the support sites with Cr(VI), and resulted in fewer adsorbance sites for Cr(VI) [33]. Therefore, it is better to first eliminate the coexisting SO_4^{2-} and Ca^{2+} to acquire a relatively high removal efficiency of MBTS for Cr(VI) adsorption.
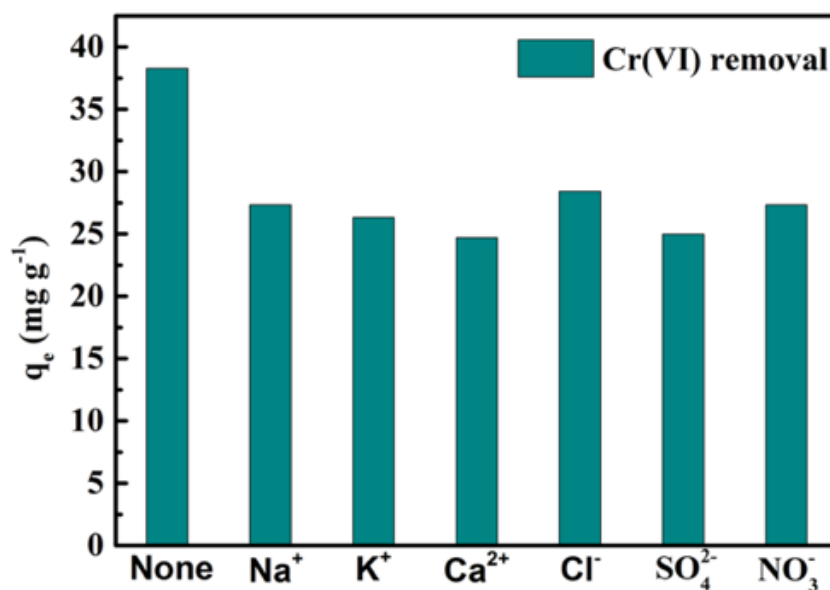
Figure 6. Effect of initial coexisting ion value on the removal of Cr(VI). (I = 0.01 M, pH = 3.0 ± 0.1, T = 298 K).

3.5. Adsorption Mechanism

To investigate the adsorption mechanism between Cr(VI) and MBTS, XPS were supplied with MBTS before and after Cr(VI) adsorption. XPS technology could supply both element analysis and chemical valence changes [42]. As shown in Figure 7a, four major elements are found on MBTS, including C1s, N1s, O1s, and Fe2p. The high-resolution spectrum of Cr2p revealed that Cr element peaks were detected on the after-adsorption spectra, which showed that the chromium adsorbed on the MBTS surface successfully, in comparison with the spectra before adsorption. According to the spectrum of Fe2p (Figure 7e), two characteristic valences of MBTS revealed by XPS result could be peaked at 724.14 eV (Fe2p$_{1/2}$) and 711.3 eV (Fe2p$_{3/2}$) binding energy that was assigned to Fe$_3$O$_4$ [43], which matched with the XRD results. The resolution of C1s showed four kinds of carbon atoms on MBTS. The peak at 283.45 eV could be assigned to the C–C bond [44], the peak at 284.8 eV was non-oxygenated carbon (C–N bond), the peak at 286.21 eV was a C–O bond, and the peak in 290.43eV was a carboxylate carbon (O–C=O bond) [45], demonstrating that MBTS abounded with oxygen functional groups and C–O binding energy appeared after adsorption. Regarding the O1s, there are three various oxygen-containing functional groups: (a) COOH, 535.07 eV, (b) O-H, 533.41 eV, and (c) C=O, 531.20 eV. It was found that the peak of O–H transformed into 531.84 eV and the intensities of O–the H peaks had a slight decrease after Cr(VI) adsorption. Meanwhile, the peaks at 531.20 eV converted to 530.1 eV, which represented Fe-O functional group [45] becoming significantly higher, meaning that the hydroxyl groups were partially replaced by HCrO$_4^-$/Cr$_2$O$_7^{2-}$ [46]. The Cr2p spectrum of MBTS showed that Cr2p$_{3/2}$ and Cr2p$_{1/2}$ peaks were situated at 587.26 eV and 578.86 eV, which were characteristic of Cr(VI) and Cr(III). Additionally, the existence of Cr(III) indicated that the Cr(VI) adsorbed on the surface of MBTS, then deoxidated to Cr(III). Figure 7c shows the N1s peaks assigning to the peaks at 398.9 eV for -NH- and 401.8.9 eV for -N=(-C=NH), which were quinoid imine units and benzenoid amine units [47]. After adsorption, a new peak emerged at 400.73 eV for -N=$^+$, which should be H$^+$ doped on -N=. This is in accordance with the pH increase after adsorption (Figure 5, when the pH of Cr solution < 6), indicating that the protonation promotes the consumption of H$^+$. Furthermore, Cr(III) doped on MBTS might be another reason for the production of -NH=$^+$. From the above analysis and the experimental results, it can be determined that the removal of Cr(VI) could be dominated by three steps: (1) Cr(VI) exchanged with hydroxyl groups on MBTS; (2) the Cr(VI) adsorbed on MBTS was reduced to Cr(III); and (3) the chelation reaction

between Cr(III) and amino groups of MBTS. The responsible groups for the reduction in Cr(VI) to Cr(III) are shown below in Equation (9) to Equation (13) [35,48].
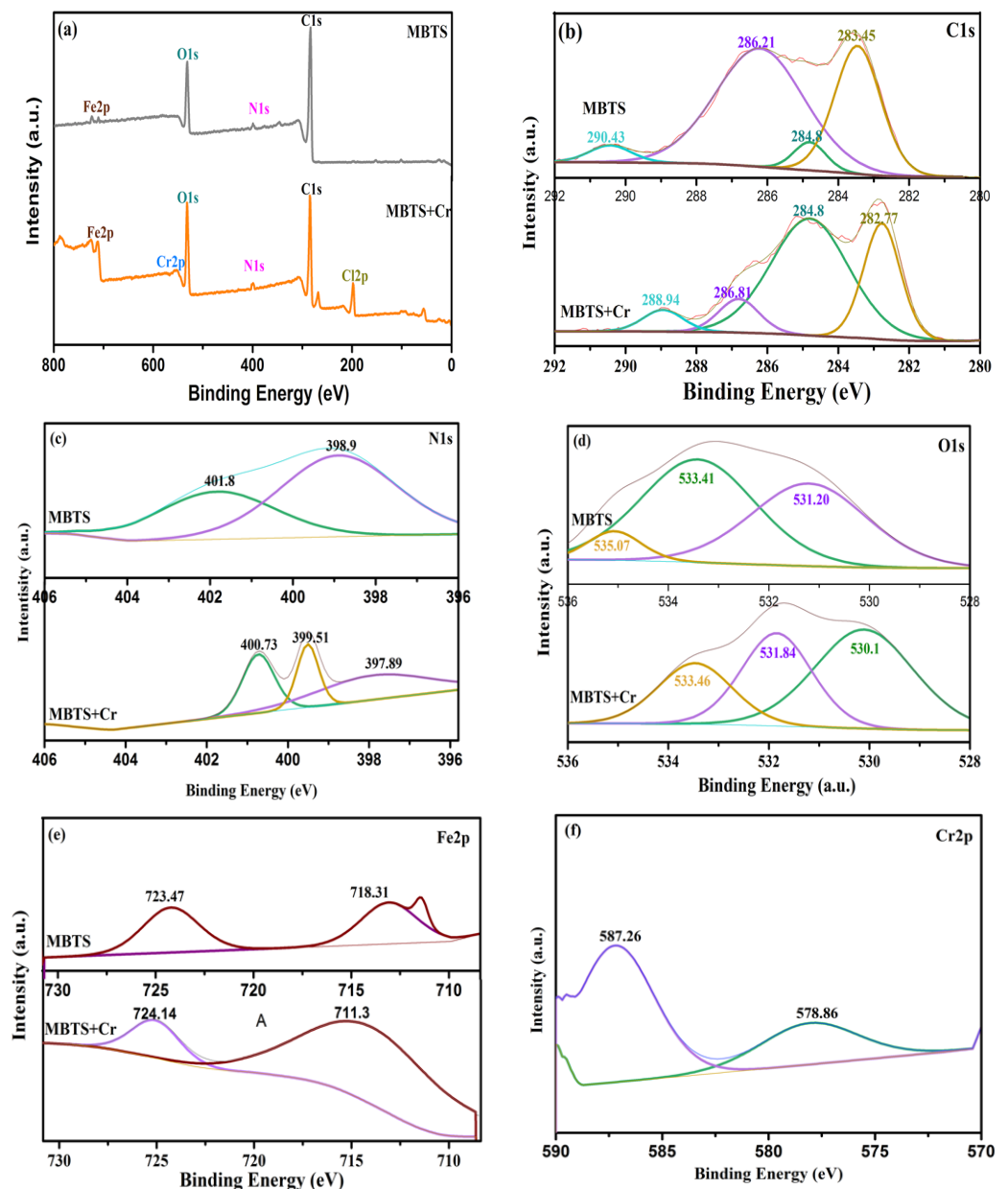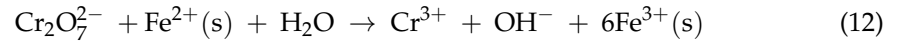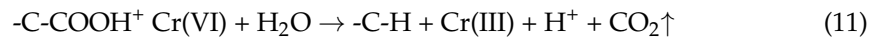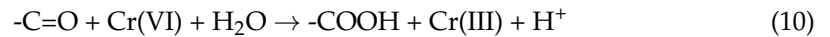
$$-C\text{-}H + Cr(VI) + H_2O \rightarrow \text{-}C\text{-}OH + Cr(III) + H^+ \tag{9}$$

$$-C\text{=}O + Cr(VI) + H_2O \rightarrow \text{-}COOH + Cr(III) + H^+ \tag{10}$$

$$-C\text{-}COOH^+ Cr(VI) + H_2O \rightarrow \text{-}C\text{-}H + Cr(III) + H^+ + CO_2\uparrow \tag{11}$$

$$Cr_2O_7^{2-} + Fe^{2+}(s) + H_2O \rightarrow Cr^{3+} + OH^- + 6Fe^{3+}(s) \tag{12}$$

$$\text{Surface C }(+) + Cr_2O_7^{2-} \rightarrow \text{Surface C} - Cr_2O_7 \text{ (Surface)} \tag{13}$$
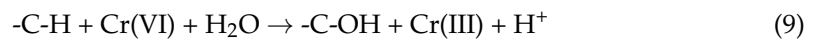

Figure 7. (**a**) XPS spectra; (**b–e**) C1s, N1s, O1s, and Fe2p spectra of MBTS before and after adsorption; and (**f**) Cr2p of MBTS.

3.6. Engineering Implication

As the main residue of tobacco cultivation, the treatment focused on incineration, landfill, or allowed for decomposition [49], which poses a great burden and pollution to the

environment. Additionally, the tobacco stems were added to stoves for heating or cooking but had just a 10% burning efficiency [50]. Tobacco stems are a precious and valuable resource. Some studies have shown that biochar derived from tobacco stems had a better effect in treating heavy metals in wastewater and improving soil amendment [51–53]. The preparation of tobacco stems into biochar enhanced its own added value and could be applied in the industry. However, to the best of the author's knowledge, this was the first time that the modified biochar made from tobacco stems was found to have a high adsorption activity for hexavalent chromium. Through modification, the Cr(VI) adsorption capacity evidently improved, reaching a 15 time higher capacity than the raw tobacco stem biochar in this study. Therefore, biochar derived from tobacco stems modified by Fe_3O_4 magnetic particles could be used for the treatment of chromium-contaminated wastewater, thus achieving the purpose of waste disposal and becoming more economical (Figure 8). This concept was in accordance with the circular economy conception for potential metal-polluted wastewater treatment.
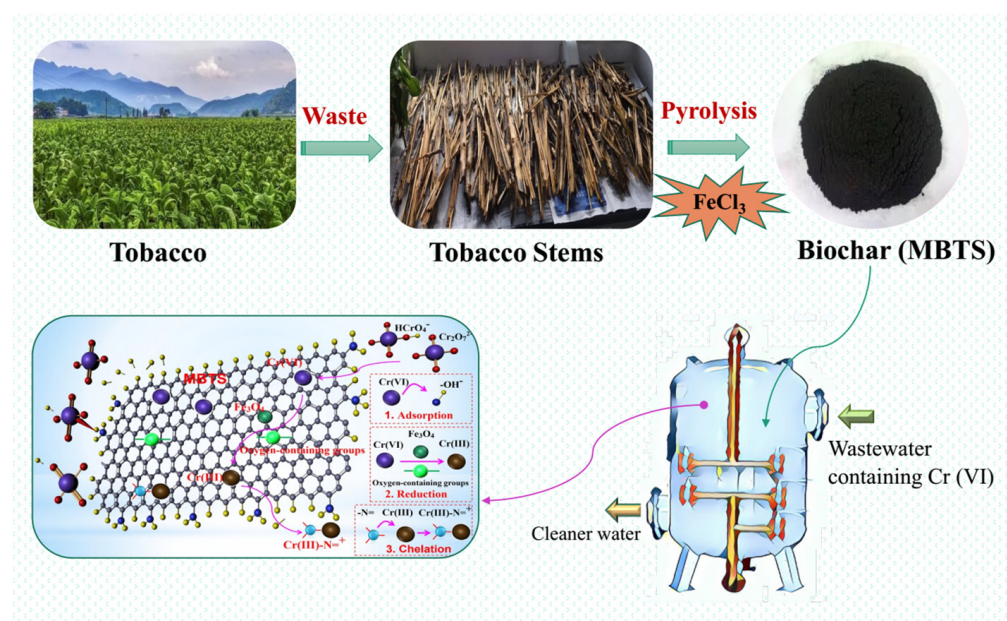

Figure 8. The engineering implication and mechanism of MBTS on Cr(VI) removal.

4. Conclusions

In this work, new magnetic biochar originated from a burley tobacco stem (MBTS) was fit for Cr(VI) removal. The optimization conditions for the sample preparation were pyrolysis at 400 °C for 1h and a mass ratio of Fe: MBTS of 0.5. Through the modification of ferric ion, MBTS contained abundant function groups (C–H, C=N, and C=O). Both the pH and coexisted ions had an important influence on the removal of Cr(VI). The Cr(VI) removal mechanism followed by three steps: Cr(VI) was reduced to Cr(III), after it was adsorbed and exchanged OH with MBTS; then, Cr(III) produced a complex reaction with the amino groups of MBTS. The novel biochar material showed an outstanding Cr(VI) removal capacity, and the maximum adsorption capacity of MBTS was 58.74 mg/g, much higher than burley tobacco stem biochar (BTS). Therefore, the MBTS prepared in this study has a prospective application for removing Cr(VI) from contaminated water.

Author Contributions: Conceptualization, W.L., B.C. and Y.L.; software, Z.C., D.G. and Z.Z.; data curation and writing—original draft preparation, B.C.; writing—review and editing, Y.L.; visualization, F.W. and Y.D.; supervision and funding acquisition, W.L. All authors have read and agreed to the published version of the manuscript.

Data Availability Statement: Not applicable.

Conflicts of Interest: The authors declare no conflict of interest.

References

1. Miretzky, P.; Cirelli, A.F. Cr(VI) and Cr(III) removal from aqueous solution by raw and modified lignocellulosic materials: A review. *J. Hazard. Mater.* **2010**, *180*, 1–19. [CrossRef] [PubMed]
2. Chen, Y.; Ma, J.; Miao, C.; Ruan, X. Occurrence and environmental impact of industrial agglomeration on regional soil heavy metalloid accumulation: A case study of the Zhengzhou Economic and Technological Development Zone (ZETZ), China. *J. Clean. Prod.* **2020**, *245*, 118676. [CrossRef]
3. Pan, Z.; Zhu, X.; Satpathy, A.; Li, W.; Fortner, J.D.; Giammar, D.E. Cr(VI) Adsorption on Engineered Iron Oxide Nanoparticles: Exploring Complexation Processes and Water Chemistry. *Environ. Sci. Technol.* **2019**, *53*, 11913–11921. [CrossRef] [PubMed]
4. Guo, D.; Li, Y.; Cui, B.; Hu, M.; Luo, S.; Ji, B.; Liu, Y. Natural adsorption of methylene blue by waste fallen leaves of Magnoliaceae and its repeated thermal regeneration for reuse. *J. Clean. Prod.* **2020**, *267*, 121903. [CrossRef]
5. Shi, Y.; Shan, R.; Lu, L.; Yuan, H.; Jiang, H.; Zhang, Y.; Chen, Y. High-efficiency removal of Cr(VI) by modified biochar derived from glue residue. *J. Clean. Prod.* **2020**, *254*, 119935. [CrossRef]
6. Shu, Y.; Ji, B.; Cui, B.; Shi, Y.; Wang, J.; Hu, M.; Luo, S.; Guo, D. Almond Shell-Derived, Biochar-Supported, Nano-Zero-Valent Iron Composite for Aqueous Hexavalent Chromium Removal: Performance and Mechanisms. *Nanomaterials* **2020**, *10*, 198. [CrossRef]
7. Cui, B.; Chen, Z.; Guo, D.; Liu, Y. Investigations on the pyrolysis of microalgal-bacterial granular sludge: Products, kinetics, and potential mechanisms. *Bioresour. Technol.* **2021**, *349*, 126328. [CrossRef]
8. Yang, J.; Ji, G.; Gao, Y.; Fu, W.; Irfan, M.; Mu, L.; Zhang, Y.; Li, A. High-yield and high-performance porous biochar produced from pyrolysis of peanut shell with low-dose ammonium polyphosphate for chloramphenicol adsorption. *J. Clean. Prod.* **2020**, *264*, 121516. [CrossRef]
9. Yu, Y.; An, Q.; Jin, L.; Luo, N.; Li, Z.; Jiang, J. Unraveling sorption of Cr(VI) from aqueous solution by FeCl3 and ZnCl2-modified corn stalks biochar: Implicit mechanism and application. *Bioresour. Technol.* **2020**, *297*, 122466. [CrossRef]
10. Deng, J.; Li, X.; Wei, X.; Liu, Y.; Liang, J.; Shao, Y.; Huang, W.; Cheng, X. Different adsorption behaviors and mechanisms of a novel amino-functionalized hydrothermal biochar for hexavalent chromium and pentavalent antimony. *Bioresour. Technol.* **2020**, *310*, 123438. [CrossRef]
11. Kasozi, G.N.; Zimmerman, A.R.; Nkedi-Kizza, P.; Gao, B. Catechol and Humic Acid Sorption onto a Range of Laboratory-Produced Black Carbons (Biochars). *Environ. Sci. Technol.* **2010**, *44*, 6189–6195. [CrossRef] [PubMed]
12. Liu, L.; Liu, X.; Wang, D.; Lin, H.; Huang, L. Removal and reduction of Cr(VI) in simulated wastewater using magnetic biochar prepared by co-pyrolysis of nano-zero-valent iron and sewage sludge. *J. Clean. Prod.* **2020**, *257*, 120562. [CrossRef]
13. Dong, X.; Ma, L.Q.; Li, Y. Characteristics and mechanisms of hexavalent chromium removal by biochar from sugar beet tailing. *J. Hazard. Mater.* **2011**, *190*, 909–915. [CrossRef] [PubMed]
14. Li, Y.; Xing, B.; Ding, Y.; Han, X.; Wang, S. A critical review of the production and advanced utilization of biochar via selective pyrolysis of lignocellulosic biomass. *Bioresour. Technol.* **2020**, *312*, 123614. [CrossRef]
15. Roberts, K.G.; Gloy, B.A.; Joseph, S.; Scott, N.R.; Lehmann, J. Life cycle assessment of biochar systems- estimating the energetic, economic, and climate change potential. *Environ. Sci. Technol.* **2010**, *44*, 827–833. [CrossRef]
16. El-Azazy, M.; Nabil, I.; Hassan, S.S.; El-Shafie, A.S. Adsorption Characteristics of Pristine and Magnetic Olive Stones Biochar with Respect to Clofazimine. *Nanomaterials* **2021**, *11*, 963. [CrossRef]
17. Jia, Y.; Wang, Y.; Zhang, Q.; Rong, H.; Liu, Y.; Xiao, B.; Guo, D.; Laghari, M.; Ruan, R. Gas-carrying enhances the combustion temperature of the biomass particles. *Energy* **2022**, *239*, 121956. [CrossRef]
18. Chen, R.; Li, L.; Liu, Z.; Lu, M.; Wang, C.; Li, H.; Ma, W.; Wang, S. Preparation and characterization of activated carbons from tobacco stem by chemical activation. *J. Air Waste Manag. Assoc.* **2017**, *67*, 713–724. [CrossRef]
19. Zhang, J.; Zhang, J.; Wang, M.; Wu, S.; Wang, H.; Niazi, N.K.; Man, Y.B.; Christie, P.; Shan, S.; Wong, M.H. Effect of tobacco stem-derived biochar on soil metal immobilization and the cultivation of tobacco plant. *J. Soils Sediments* **2019**, *19*, 2313–2321. [CrossRef]
20. Mumba, P.; Phiri, R. Environmental impact assessment of tobacco waste disposal. *Int. J. Environ. Res.* **2008**, *2*, 225–230.
21. Trubetskaya, A.; Kling, J.; Ershag, O.; Attard, T.M.; Schroder, E. Removal of phenol and chlorine from wastewater using steam activated biomass soot and tire carbon black. *J. Hazard. Mater.* **2019**, *365*, 846–856. [CrossRef]
22. Singh, U.K.; Kumar, B. Pathways of heavy metals contamination and associated human health risk in Ajay River basin, India. *Chemosphere* **2017**, *174*, 183–199. [CrossRef] [PubMed]
23. Shan, D.; Deng, S.; Zhao, T.; Wang, B.; Wang, Y.; Huang, J.; Yu, G.; Winglee, J.; Wiesner, M.R. Preparation of ultrafine magnetic biochar and activated carbon for pharmaceutical adsorption and subsequent degradation by ball milling. *J. Hazard. Mater.* **2016**, *305*, 156–163. [CrossRef] [PubMed]
24. Zhu, J.; Wei, S.; Gu, H.; Rapole, S.B.; Wang, Q.; Luo, Z.; Haldolaarachchige, N.; Young, D.P.; Guo, Z. One-pot synthesis of magnetic graphene nanocomposites decorated with core@double-shell nanoparticles for fast chromium removal. *Environ. Sci. Technol.* **2012**, *46*, 977–985. [CrossRef]

25. Anirudhan, T.S.; Senan, P. Adsorptive Characteristics of Chromium(VI) Ions from Aqueous Phase by Iron(III) Coordinated Amino-Functionalized Poly(glycidyl methacrylate)-Grafted Cellulose: Equilibrium Kinetics and Thermodynamic Study. *Sep. Sci. Technol.* **2011**, *46*, 1430–1442. [CrossRef]
26. He, J.; Long, Y.; Wang, Y.; Wei, C.; Zhan, J. Aerosol-Assisted Self-Assembly of Reticulated N-Doped Carbonaceous Submicron Spheres for Effective Removal of Hexavalent Chromium. *ACS Appl. Mater. Interfaces* **2016**, *8*, 16699–16707. [CrossRef] [PubMed]
27. Ooi, F.; DuChene, J.S.; Qiu, J.; Graham, J.O.; Engelhard, M.H.; Cao, G.; Gai, Z.; Wei, W.D. A Facile Solvothermal Synthesis of Octahedral Fe3 O4 Nanoparticles. *Small* **2015**, *11*, 2649–2653. [CrossRef]
28. Shi, S.; Yang, J.; Liang, S.; Li, M.; Gan, Q.; Xiao, K.; Hu, J. Enhanced Cr(VI) removal from acidic solutions using biochar modified by Fe3O4@SiO2-NH2 particles. *Sci. Total Environ.* **2018**, *628–629*, 499–508. [CrossRef]
29. Typical IR Absorption Frequencies For Common Functional Groups. Available online: https://www.niu.edu/clas/chembio/research/analytical-lab/ftir/ir-frequencies-table.shtml (accessed on 31 December 2021).
30. The Nature of Vibrational Spectroscopy. Available online: https://www2.chemistry.msu.edu/faculty/reusch/virttxtjml/spectrpy/infrared/irspec1.htm (accessed on 31 December 2021).
31. Sha, O.; Wang, Y.; Yin, X.; Chen, X.; Chen, L.; Wang, S. Magnetic Solid-Phase Extraction Using Fe3O4@SiO2 Magnetic Nanoparticles Followed by UV-Vis Spectrometry for Determination of Paraquat in Plasma and Urine Samples. *J. Anal. Methods Chem.* **2017**, *2017*, 8704639. [CrossRef]
32. Zhang, X.; Liu, Y. Ultrafast removal of radioactive strontium ions from contaminated wastewater by nanostructured layered sodium vanadosilicate with high adsorption capacity and selectivity. *J. Hazard. Mater.* **2020**, *398*, 122907. [CrossRef]
33. He, R.; Yuan, X.; Huang, Z.; Wang, H.; Jiang, L.; Huang, J.; Tan, M.; Li, H. Activated biochar with iron-loading and its application in removing Cr(VI) from aqueous solution. *Colloids Surf. A Physicochem. Eng. Asp.* **2019**, *579*, 123642. [CrossRef]
34. Zou, H.; Zhao, J.; He, F.; Zhong, Z.; Huang, J.; Zheng, Y.; Zhang, Y.; Yang, Y.; Yu, F.; Bashir, M.A.; et al. Ball milling biochar iron oxide composites for the removal of chromium (Cr(VI)) from water: Performance and mechanisms. *J. Hazard. Mater.* **2021**, *413*, 125252. [CrossRef] [PubMed]
35. Zhuang, L.; Li, Q.; Chen, J.; Ma, B.; Chen, S. Carbothermal preparation of porous carbon-encapsulated iron composite for the removal of trace hexavalent chromium. *Chem. Eng. J.* **2014**, *253*, 24–33. [CrossRef]
36. Liu, Y. Is the Free Energy Change of Adsorption Correctly Calculated? *J. Chem. Eng.* **2009**, *84*, 1981–1985. [CrossRef]
37. Gao, M.; Wang, X.; Xia, C.; Song, N.; Ma, Y.; Wang, Q.; Yang, T.; Ge, S.; Wu, C.; Lam, S.S. Phenol removal via activated carbon from co-pyrolysis of waste coal tar pitch and vinasse. *Korean J. Chem. Eng.* **2021**, *38*, 64–71. [CrossRef]
38. Li, Y.; Zhu, S.; Liu, Q.; Chen, Z.; Gu, J.; Zhu, C.; Lu, T.; Zhang, D.; Ma, J. N-doped porous carbon with magnetic particles formed in situ for enhanced Cr(VI) removal. *Water Res.* **2013**, *47*, 4188–4197. [CrossRef]
39. Zhang, X.; Lv, L.; Qin, Y.; Xu, M.; Jia, X.; Chen, Z. Removal of aqueous Cr(VI) by a magnetic biochar derived from Melia azedarach wood. *Bioresour. Technol.* **2018**, *256*, 1–10. [CrossRef]
40. Shi, Y.; Zhang, T.; Ren, H.; Kruse, A.; Cui, R. Polyethylene imine modified hydrochar adsorption for chromium (VI) and nickel (II) removal from aqueous solution. *Bioresour. Technol.* **2018**, *247*, 370–379. [CrossRef]
41. Gollavelli, G.; Chang, C.-C.; Ling, Y.-C. Facile Synthesis of Smart Magnetic Graphene for Safe Drinking Water: Heavy Metal Removal and Disinfection Control. *ACS Sustain. Chem. Eng.* **2013**, *1*, 462–472. [CrossRef]
42. Qi, W.; Zhao, Y.; Zheng, X.; Ji, M.; Zhang, Z. Adsorption behavior and mechanism of Cr(VI) using Sakura waste from aqueous solution. *Appl. Surf. Sci.* **2016**, *360*, 470–476. [CrossRef]
43. Ding, X.; Xiao, D.; Ji, L.; Jin, D.; Dai, K.; Yang, Z.; Wang, Z.; Chen, H. Simple fabrication of Fe3O4:C:gC3N4 two-dimensional composite by hydrothermal carbonization approach with enhanced photocatalytic performance under visible light. *Catal. Sci. Technol.* **2018**, *8*, 3484–3492. [CrossRef]
44. Smith, M.; Scudiero, L.; Espinal, J.; McEwen, J.-S.; Garcia-Perez, M. Improving the deconvolution and interpretation of XPS spectra from chars by ab initio calculations. *Carbon* **2016**, *110*, 155–171. [CrossRef]
45. Wen, T.; Wang, J.; Yu, S.; Chen, Z.; Hayat, T.; Wang, X. Magnetic Porous Carbonaceous Material Produced from Tea Waste for Efficient Removal of As(V), Cr(VI), Humic Acid, and Dyes. *ACS Sustain. Chem. Eng.* **2017**, *5*, 4371–4380. [CrossRef]
46. Cao, C.Y.; Qu, J.; Yan, W.S.; Zhu, J.F.; Wu, Z.Y.; Song, W.G. Low-cost synthesis of flowerlike alpha-Fe2O3 nanostructures for heavy metal ion removal: Adsorption property and mechanism. *Langmuir* **2012**, *28*, 4573–4579. [CrossRef]
47. Wang, T.; Zhang, L.; Li, C.; Yang, W.; Song, T.; Tang, C.; Meng, Y.; Dai, S.; Wang, H.; Chai, L.; et al. Synthesis of Core-Shell Magnetic Fe3O4@poly(m-Phenylenediamine) Particles for Chromium Reduction and Adsorption. *Environ. Sci. Technol.* **2015**, *49*, 5654–5662. [CrossRef]
48. Su, C.; Wang, S.; Zhou, Z.; Wang, H.; Xie, X.; Yang, Y.; Feng, Y.; Liu, W.; Liu, P. Chemical processes of Cr(VI) removal by Fe-modified biochar under aerobic and anaerobic conditions and mechanism characterization under aerobic conditions using synchrotron-related techniques. *Sci. Total Environ.* **2021**, *768*, 144604. [CrossRef]
49. He, H.; Zhang, N.; Chen, N.; Lei, Z.; Shimizu, K.; Zhang, Z. Efficient phosphate removal from wastewater by MgAl-LDHs modified hydrochar derived from tobacco stalk. *Bioresour. Technol. Rep.* **2019**, *8*, 100348. [CrossRef]
50. Qin, Z.; Sun, M.; Luo, X.; Zhang, H.; Xie, J.; Chen, H.; Yang, L.; Shi, L. Life-cycle assessment of tobacco stalk utilization. *Bioresour. Technol.* **2018**, *265*, 119–127. [CrossRef]
51. Chen, R.; Zhang, J.; Lun, L.; Li, Q.; Zhang, Y. Comparative study on synergistic effects in co-pyrolysis of tobacco stalk with polymer wastes: Thermal behavior, gas formation, and kinetics. *Bioresour. Technol.* **2019**, *292*, 121970. [CrossRef]

52. Zhou, N.; Zu, J.; Feng, Q.; Chen, H.; Li, J.; Zhong, M.-E.; Zhou, Z.; Zhuang, S. Effect of pyrolysis condition on the adsorption mechanism of heavy metals on tobacco stem biochar in competitive mode. *Environ. Sci. Pollut. Res.* **2019**, *26*, 26947–26962. [CrossRef]
53. Lahori, A.H.; Zhang, Z.; Shaheen, S.M.; Rinklebe, J.; Guo, Z.; Li, R.; Mahar, A.; Wang, Z.; Ren, C.; Mi, S.; et al. Mono-and co-applications of Ca-bentonite with zeolite, Ca-hydroxide, and tobacco biochar affect phytoavailability and uptake of copper and lead in a gold mine-polluted soil. *J. Hazard. Mater.* **2019**, *374*, 401–411. [CrossRef] [PubMed]